Numerical modeling of concrete flow: homogeneous approach

Frédéric Dufour, Gilles Pijaudier-Cabot

Numerical modelling of concrete flow: homogeneous approach

Frédéric Dufour and Gilles Pijaudier-Cabot

R&DO, GeM, Institut de Recherche en génie civil et mécanique, Ecole Centrale de Nantes, Université de Nantes, CNRS, 1 rue de la Noë, BP 92101, F-44321 Nantes Cedex 3, France

The aim of this paper is to model numerically concrete flow inside formworks like the Lbox. For this purpose, we use a finite element method with Lagrangian integration points (FEMLIP). We are able to follow in time and space material motion with any type of material behaviour, including non-linear and time-dependent ones. We also can deal with free surfaces or material interfaces. Bingham's rheology is used for fresh concrete behaviour. In order to compare with experiments, we have considered three concretes (OC, HPC and SCC) with contrasted rheologies. Their yield stress is identified by experimental slump tests and also compared with the value given by a formulation concrete software. Experimental data are found to be quite close to numerical predictions. We have also made some experimental flow tests in a LBOX. We measured the flow speed and the flow shape in the final stage. The numerical modelling of these experiments is very encouraging and shows the capability of the FEMLIP using the Bingham's law to model concrete flow and filling properties.

KEY WORDS: numerical modelling; fresh concrete flow; Bingham's model; finite element method with Lagrangian integration points

1. INTRODUCTION

Many problems of durability of concrete structures are due to bad filling of formworks. This issue is increasing year after year as formworks are getting more and more complex and reinforcements are getting denser and denser with the use of high performance concretes (HPC) with a high workability and self-compacting concretes (SCC). As for aesthetic aspects, it is most of the time only a matter of cost as the surface can be retrofitted afterwards. Unfortunately, if problems such as segregation of aggregates occur inside the structure, they cannot be detected easily. This may happen for tortuous formworks and/or around reinforcement bars due to locking problems. Even if no voids are formed during the filling, segregation may still occur which yields a heterogeneous hardened material at the scale of the structure. In this case, the durability of the structure may be endangered as transfer properties of concrete are increased or

Correspondence to: F. Dufour, R&DO, GeM, Institut de Recherche en génie civil et mécanique, Ecole Centrale de Nantes, BP 92101, 44321, Nantes Cedex 3, France.
E-mail: Frederic.Dufour@ec-nantes.fr
E-mail: Gilles.Pijaudier-Cabot@ec-nantes.fr

the steel concrete interface mechanical properties are decreased. It is therefore of importance to devise numerical tools aimed at the simulation of the filling of formworks with concrete. This paper is a first step toward this goal. It addresses the numerical modelling of concrete flow, assuming that concrete is homogeneous but the material modelling and the numerical method can easily be applied to the simulation of heterogeneous fluids (see e.g. Reference [1]).

Among the difficulties of the simulation of concrete flow, the numerical aspects and the identification of the concrete rheology parameters are those addressed in this paper where we model fresh concrete as a homogeneous viscous fluid. On the material side, tests, as simple as possible, are required in order to calibrate the model parameters. On the numerical side, we need to follow in time and space the flow of concrete with moving free surfaces. A purely Eulerian finite element method cannot easily handle the tracking of free surfaces and material interfaces when aggregates are modelled explicitly. On the contrary with heterogeneous materials, it is natural to deal with a Lagrangian description in the finite element description, but unfortunately not for very large deformation processes. The discrete element method (DEM) has also been used by Petersson [2] and Noor and Uomoto [3]. Even if large deformations are natural for DEM, inter-particle properties are not easy to identify. Very often, a trial and error approach is needed for that, and it is not really compatible with the large amount of computational time needed per run.

In the present paper, we use a finite element method with Lagrangian integration points (FEMLIP). This method has already shown a great potential [1, 4] in geophysics. We focus here on the numerical aspect of concrete flow modelling. In the first section, we describe the numerical code and discuss the rheological models for concrete. In the second part, we calibrate Bingham's parameters on experimental tests and compare them with values given by a formulation concrete software named *Bétonlab*. Finally, we compare numerical results on LBOX flow against experimental results.

2. NUMERICAL MODELLING

2.1. Constitutive equations

Concrete, in its fresh state, can be considered as a fluid, provided that a certain degree of flow can be achieved and that the mix is quasi-homogeneous with regularly dispersed aggregate particles (in space and size). Modelling concrete rheology is a very difficult task as every concrete behaves differently depending on their composition and mixing method. Therefore, it is impossible to write a relation between the stress and the strain rate based on every single parameter at the microscale, namely quantities and nature of each admixtures which are nowadays more and more numerous. Here, the concrete rheology is thought at a mesoscale and it is written as a relation between the shear stress τ and the shear strain rate $\dot{\gamma}$. A complete review of rheological models for cement-based materials has been done by Yahia and Khayat [5]. We discuss here only the three simplest ones, namely Newton's, Bingham's and Herschel–Bulkley's models.

The simplest model (one parameter) assumes that concrete is a Newtonian fluid

$$\tau = \eta\dot{\gamma} \tag{1}$$

where η is the viscosity but Tatersall [6] has shown that a single parameter is not enough to model concrete flow. At least two parameters are needed to model concrete with a slump at the Abrams cone test lower than 30 cm. The first one needs to be related to the static behaviour (slump test) and the second one to the dynamic fluid response (rheometer test). Hence, a stress threshold has been added to the Newton's model to give the Bingham's model:

$$\begin{aligned} \tau &= \tau_0 + \eta\dot{\gamma} \quad \text{if } \tau \geqslant \tau_0 \\ \dot{\gamma} &= 0 \quad \text{if } \tau \leqslant \tau_0 \end{aligned} \tag{2}$$

where τ_0 is the yield stress and η is the plastic viscosity.

When experimental data are fitted for many different concretes and for self-compacting concrete especially, it often yields a negative value of the yield stress although very small. For this reason de Larrard *et al.* [7] preferred to use a Herschel–Bulkley's model (3 parameters):

$$\tau = \tau_0' + a\dot{\gamma}^b \tag{3}$$

The same authors [8] propose a method to keep using the simpler Bingham's model. Instead of deducting the Bingham's curve directly from experimental results using a least square method, a Herschel–Bulkley curve is fitted on experimental results as a first step and then, the Bingham's curve is deducted from the Herschel–Bulkley curve with a least square method. This method keeps the yield stress τ_0 unchanged for both models and computes the plastic viscosity for the Bingham's model as follows:

$$\eta = \frac{3a}{b+2}\dot{\gamma}_{\max}^{b-1} \tag{4}$$

where $\dot{\gamma}_{\max}$ is the maximum shear strain rate applied to the sample during test (usually $\dot{\gamma}_{\max} = 6\ \mathrm{s}^{-1}$). One example for each rheological model is plotted in Figure 1.

Ferraris and de Larrard [8] have found a mean value for b of 1.53 for concrete without superplasticizer and 1.36 for others. The Bingham's model (e.g. $b = 1$) is most widely used [9] because it needs less experimental tests to be calibrated. For the same reason, we have chosen to use the Bingham's model in this study where three different concretes will be represented.

For an easier numerical implementation, the Bingham's model needs to be smoothed [10] in order to avoid the sharp angle at $\tau = \tau_0$ on the material response and the use of two equations below and above the shear stress threshold. This yields

$$\eta = \eta_0 + \frac{\tau_0}{\dot{\gamma}}(1 - \mathrm{e}^{-m\dot{\gamma}}) \tag{5}$$

where m is the stress growth rate parameter. The higher m, the more accurate the approximation. We found out, for the range of strain rate reached during our numerical tests, that a value $m = 5000$ is high enough as we observed no differences with results obtained with a value of $m = 10\,000$.

2.2. Mathematical model

We begin our analysis in a general way with the classical momentum conservation equation on a domain Ω bounded by Γ

$$\sigma_{ij,j} + f_i = 0 \tag{6}$$

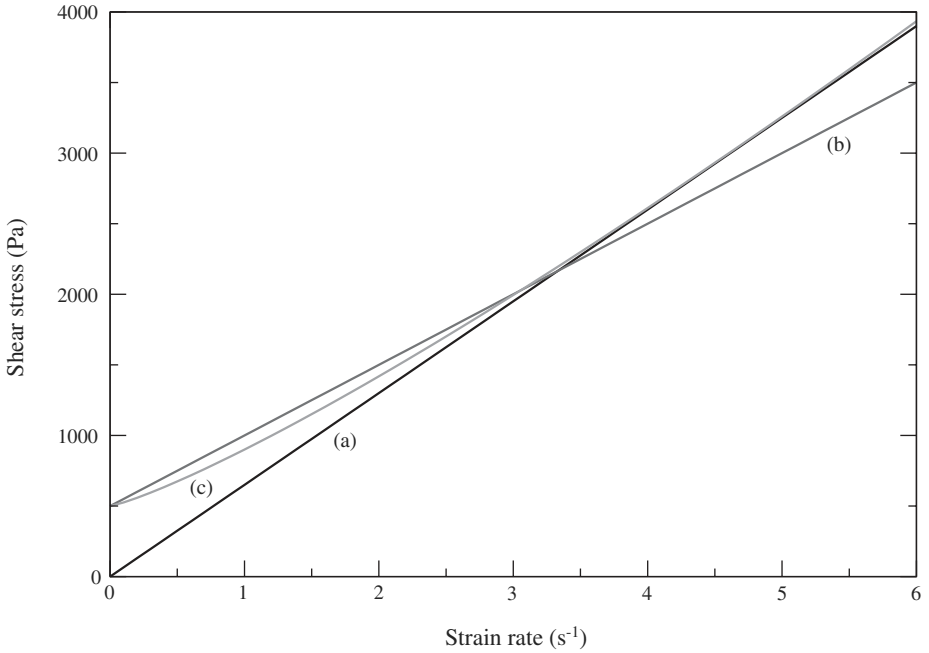

Figure 1. Different rheological models for fluid-like materials: (a) Newton ($\eta = 650$ Pa s); (b) Bingham ($\tau_0 = 500$ Pa, $\eta = 500$ Pa s); and (c) Herschel–Bulkley ($\tau_0' = 400$ Pa, $a = 500$ Pa sb and $b = 1.2$).

where $\boldsymbol{\sigma}$ is the Cauchy stress tensor and $\mathbf{f}$ is the specific body force reduced to the gravity term for concrete flow problems. The notation $\sigma_{ij,j}$ denotes the differentiation of $\boldsymbol{\sigma}$ with respect to x_j and the Einstein rules are also used for double indices. As we are only interested in very slow deformations, inertia forces are neglected in Equation (6) (infinite Prandtl number assumption). The boundary conditions are given as follows:

$$\tau_{ij} n_j - p_i = \bar{t}_i \text{ on the natural boundary } \Gamma_t \tag{7}$$

$$u_i = \bar{u}_i \text{ on the essential boundary } \Gamma_u \tag{8}$$

in which the superposed bar denotes prescribed boundary values and $\mathbf{n}$ is the unit outward normal to the domain Ω. Although concrete can be slightly dilatant [11], we assume that it is an incompressible fluid, and it is convenient to split the stress tensor into a deviatoric part $\boldsymbol{\tau}$ and an isotropic term p

$$\sigma_{ij} = \tau_{ij} - p\delta_{ij} \tag{9}$$

where p is the pressure and δ the Kronecker symbol. Equation (6) becomes

$$\tau_{ij,j} - \delta_{ij} p_{,j} + f_i = 0 \tag{10}$$

with the continuity equation

$$v_{i,i} = 0 \tag{11}$$

where $\mathbf{v}$ is the material velocity.

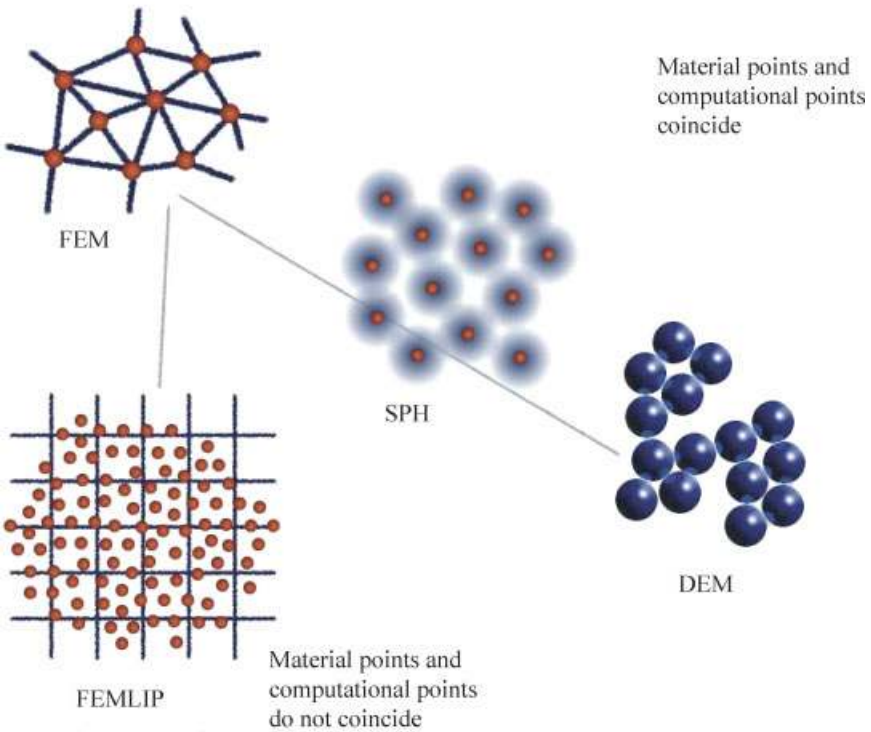

Figure 2. Different ways to discretize a problem provide a natural representation for systems with different controlling physics. In fully Lagrangian FEM, SPH and DEM all the computational points are also material points. In the FEMLIP, computational points are not materials points but a set of material points is also tracked. In ALE and Eulerian FEM there is no tracking of material points.

2.3. Numerical method

We have implemented the Bingham's model in the *ellipsis* code initially developed by Moresi and Solomatov [12]. This code is based on an Eulerian grid of finite element and a set of Lagrangian particles or tracers inside the mesh. Figure 2 presents an attempt of ranking the most used numerical methods.

Tracers carry material properties and time variables, as shown in Figure 3. This method combines the versatility and the robustness of the classical finite element method and adds a new concept of Lagrangian integration points to handle large deformation processes. At the same time, tracers may carry different material properties depending on their initial location in the finite element grid and heterogeneous structures can easily be handled [13, 14]. At each node, we solve for the velocity $\mathbf{v}$ and the pressure p, Equations (10) and (11), using tracers as integration points with a specific scheme described in Reference [13]. For computational time reasons, we have used the 2D version of *ellipsis* with bilinear elements for velocity and constant pressure elements.

For the spatial integration, we use particles instead of the classical Gaussian points. For the integration to be as accurate as with the Gaussian scheme (four integration points for bilinear

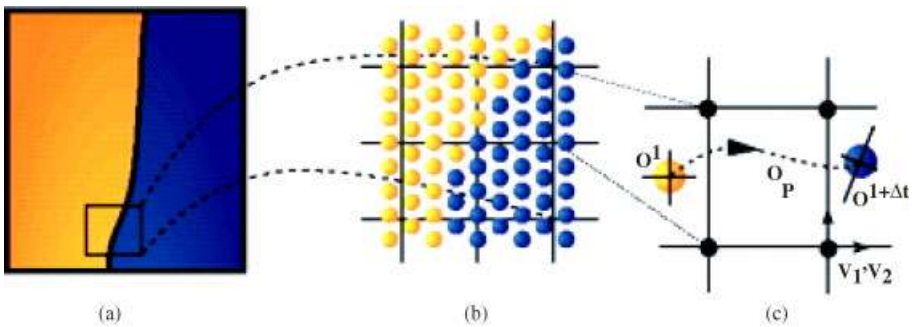

Figure 3. Summary of the FEMLIP formulation: (a) by setting different material properties onto particles one can model material interfaces; (b) the FEMLIP implies the use of more numerous particles as the integration scheme is not exact; and (c) tracers carry history variables and their position is updated according to the nodal velocity field.

solution) Moresi *et al*. [13] have shown that a minimum of 16 particles per element are needed as they may stand in any position inside the element during the flow process. One of the consequences is that the numerical weight of each particle needs to be recalculated at each timestep. At the end of each step, tracer positions are updated (Figure 3) using a Runge–Kutta time integration scheme. Tracer velocities are computed from nodal velocity field. Tracer displacements are computed according to a timestep chosen as a tracer cannot cross one element within one timestep. Contrary to the choice of the timestep for explicit schemes, our timestep is only chosen for accuracy purposes.

This method is very well suited to model fluid-like materials with interfaces and time-dependent behaviours in extremely large deformation processes. Unfortunately it has one major drawback: contrary to the Lagrangian finite element method for which only the structure of interest is discretized, the entire space occupied by the material and where it is assumed to move must be discretized. Indeed if one thinks about the Lbox problem described in Section 4, initially the material stands in the column and then it will flow down. The space where the material will flow needs to be discretized by the Eulerian grid and since each finite element needs to be filled by at least one integration point to compute nodal velocity, even if it is not accurate, it implies the use of 'air particles' to fill each finite element in which the material is supposed to flow in at any time of the computation. The same phenomenon is observed at the back of the flow where material particles leave some element empty as they flow down. Some 'air particles' have to take their place in order to keep integrating over elements. Of course those particles must have a negligible effect on the flow and therefore we set their shear strength to a negligible value compared to the strength of other particles. At the end, the major drawback yields a larger use of memory and computational time for taking into account particles, which have no effect on the flow. In the particular case of the Lbox problem, by looking at Figure 11, one can figure out that nearly 80% time and memory is used for the treatment of air particles.

2.4. Solution technique

By inserting the constitutive relation (3) into the momentum conservation equation (10) and using Equation (11), the above finite element method with moving integration points produces a

set of equations close to the one obtained with a standard finite element method:

$$\begin{pmatrix} \mathbf{K} & \mathbf{G} \\ \mathbf{G}^{\mathrm{T}} & 0 \end{pmatrix} \begin{pmatrix} \mathbf{v} \\ p \end{pmatrix} = \begin{pmatrix} \mathbf{f} \\ 0 \end{pmatrix} \tag{12}$$

where $\mathbf{K}$ is the global viscosity matrix, $\mathbf{G}$ is the discrete gradient operator. We have implemented the Uzawa scheme [15] in order to compute the velocity from one of the two equations

$$\tilde{\mathbf{K}} p = \tilde{\mathbf{f}} \tag{13}$$

$$\mathbf{G}^{\mathrm{T}} \mathbf{v} = 0 \tag{14}$$

where $\tilde{\mathbf{K}} = \mathbf{G}^{\mathrm{T}} \mathbf{K}^{-1} \mathbf{G}$ and $\tilde{\mathbf{f}} = \mathbf{G}^{\mathrm{T}} \mathbf{K}^{-1} \mathbf{f}$. We solve both equations simultaneously with a conjugate gradient operator as outlined in general in Reference [16]. Furthermore, the Eulerian grid makes it easy to use a multigrid solver for computational time savings. Indeed, computational time is proportional to the number of degree of freedom (n) whereas it is order of the square and even the cube of n for direct solver on one mesh. The main idea of multigrid schemes is to build an initial guess for an iterative solver on a coarser mesh. The scheme starts at the coarsest mesh on which it is fast to compute a solution with a direct solver. This solution is then used on the following finer mesh as an initial guess for the iterative scheme. The other main advantage of using a multigrid scheme coupled together with an iterative solver is that the first one damps out the low-frequency oscillations of the residue of Equation (12) whereas the last one damps out the high frequencies. We preferably use the full multigrid V-cycle scheme illustrated in Figure 4 as it shows good capacities for solving our type of problems. Furthermore, by experience we do not use more than five levels because the exact solution on the coarsest grid is deteriorated by going from one grid to another.

Mesh description in this paper will be given by the coarsest grid and the number of level. For further details on the complete solution technique implemented in the *ellipsis* software, the reader can refer to Moresi *et al.* [13] and Moresi and Solomatov [12].

As for any numerical scheme, one major drawback of the Gauss–Seidel iterative solver is that the convergence process becomes very slow for ill-conditioned matrix. In practice, we found out

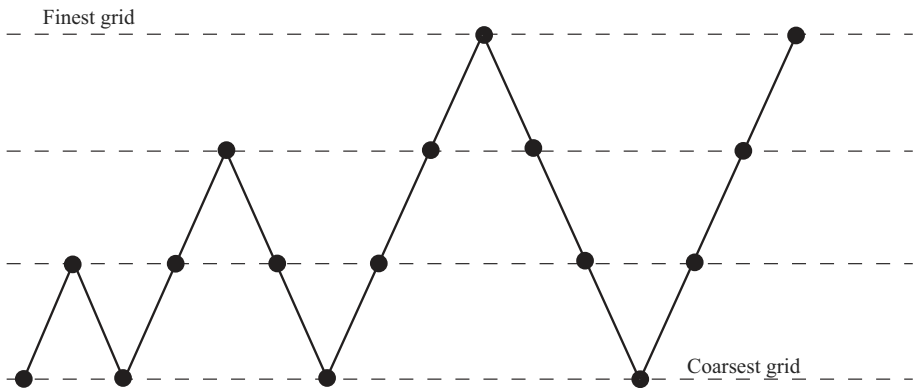

Figure 4. Example of a full multigrid V-cycle with 4 levels. Each ● is a solving process.

that we should not use a viscosity contrast (ratio of the most to the least viscous material discretized) larger than 10^4. This is quite an important issue because in our approach, 'air particles' ought to be modelled numerically. For heterogenous fluids containing aggregate particles with a very high viscosity, this may also yield more severe numerical problems, and a different solver has to be used, or the viscosity of air has to be artificially increased.

3. IDENTIFICATION OF BINGHAM'S PARAMETERS

In this section, the Bingham's parameters are identified on slump test using *ellipsis* with a trial and error approach for several concretes. The obtained modelled parameters are compared to those predicted by a concrete formulation software named *Bétonlab* [17].

3.1. Experimental study

We have formulated three different concretes in order to get three contrasted behaviours at the fresh state. One ordinary concrete (OC), one high-performance concrete (HPC) and one self-compacting concrete (SCC) are thus considered. The mix proportions of these concretes are given in Table I.

Three slump tests for each formulation have been performed on the classical axisymmetric slump cone (Figure 5(a)).

We have computed the average slump and spreading (Figure 5(b)) which are summarized in Table II. A spreading of 20 cm means that there is no motion at the base of the cone in the slump test (the specimen consolidates without any spreading of the base of the cone).

3.2. Numerical modelling

The present simulations assume a 2D (plane) fluid flow. Consequences of this assumption need to be investigated first. A 2D computation is expected to yield an approximation of the maximum shear stress value compared to a 3D approach. In order to estimate the error, we have computed the maximum shear stress with a classical finite element code on an elastic incompressible material.

We present in Table III, the results obtained according to the 2D and the axisymmetric models. We ran both models for different heights of the cone (h). From this table, we conclude that the maximum error on the shear stress between the axisymmetric model and the plane (2D)

Table I. Composition of the three different concretes.

	OC	HPC	SCC
Aggregate 6/10 (kg/m^3)	1031.3	993.6	838.7
Sand (kg/m^3)	915.2	881.7	806.3
Cement (kg/m^3)	300	360	350
Limestone filler (kg/m^3)	0	50	250
Superplasticizer (kg/m^3)	1.5	3.6	6.13
Water (kg/m^3)	193.5	186.3	197.5

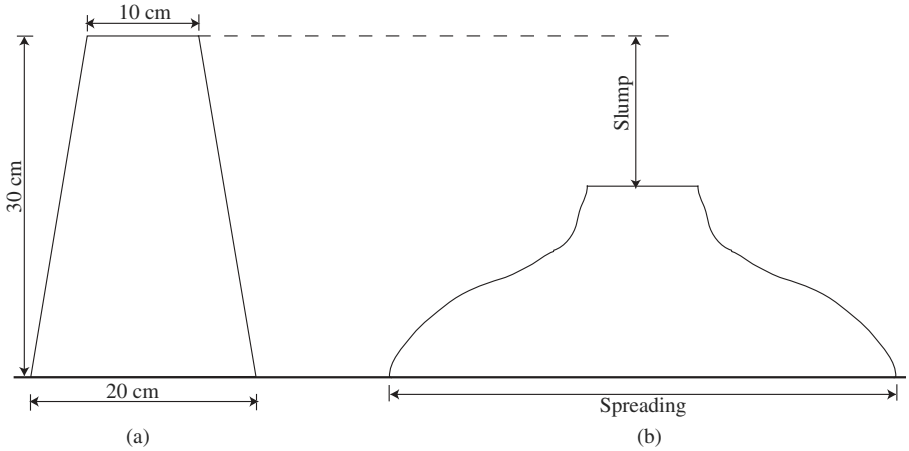

Figure 5. Geometry of the cone in the: (a) initial; and (b) final position.

Table II. Results of the slump test for each concrete.

	OC	HPC	SCC
Slump (cm)	5.5	21.5	27
Spreading (cm)	20	45	69

Table III. Comparison of maximum shear stress between 2D case and axisymmetric case.

h (cm)	Axi (Pa)	2D (Pa)	Error (%)
30	2617.7	3077.2	14.9
25	2159.7	2602.3	17
20	1775.5	2262.5	21.5
15	1333.5	1688.3	21
10	774.8	1024.8	24.4
5	314.2	467.6	32.8

model is about 17% for OC, 25% for HPC and 35% for SCC. Therefore, we expect a larger error in the identification of Bingham's parameters for SCC than for OC.

The 2D assumption does change the value of the ratio slump/spreading compared to the axisymmetric case because the material can only flow in the plane of study on the contrary of the axisymmetric model where the material can flow radially. With the same classical finite element code, we ran two sets of tests with the 2D assumption. The first set is for a given height h of the concrete cone (i.e. constant slump) and we changed the base dimension L (i.e. spreading) and the second one is for a given L, we changed h. The results are summarized in Table IV. As expected the maximum shear stress is nearly constant for a given height and various spreadings, but changes a lot for a given spreading and different heights. We conclude that with our 2D

Table IV. Comparison of maximum shear stress for different Abrams' cone geometry.

$h = 20$ cm		$L = 40$ cm	
L (cm)	τ (Pa)	h (cm)	τ (Pa)
30	2223.4	5	496.1
40	2261.1	10	1119.5
50	2247.1	15	1721.4
60	2224.3	20	2261.1
70	2198.6	25	2721
80	2173.1	30	3098.8

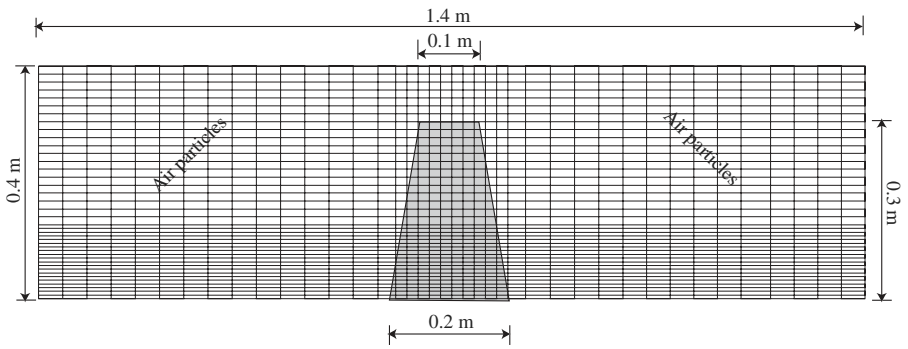

Figure 6. Mesh used in *ellipsis* for the slump test. For the sake of clarity we show the mesh at level 3. The actual finest mesh used in this work is obtained by dividing each element in 4. In the dark zone concrete particles surrounded by air particles is set.

model we may compare only slumps between experiments, which are close to an axisymmetric geometry, and the numerical model but not the base spreading which is not sensitive on the shear stress.

We used a mesh with 4 levels and 10×10 elements at the coarsest level which means 6400 elements overall. The mesh was slightly refined in the central and bottom parts where the material flow takes place (Figure 6). At least 16 particles per element are initially needed for a good estimation in the integration scheme over element, nevertheless we decided to use 36 particles per element in the concrete zone and nearby in order to define the interface between concrete and air from a geometrical point of view better. We kept a resolution of 16 particles per element in the air zone. Boundary conditions along Γ was always free-slip. It means zero shear stress and zero normal velocity. The only force term was gravity and the concrete density was estimated at 2.45.

For a very high shear strain rate, the concrete apparent viscosity tends to the plastic viscosity (order of few hundreds) and it tends to infinity as the shear strain rate tends to zero. Since we are limited to 4 orders of magnitude in the viscosity contrast between different materials (see Section 2.4) and since the behaviour of concrete contains several orders of magnitude according to the modified Bingham's model (5), it is interesting to modify the air particle viscosity during the flow. At each time step, the minimum viscosity over the concrete particles is computed and we

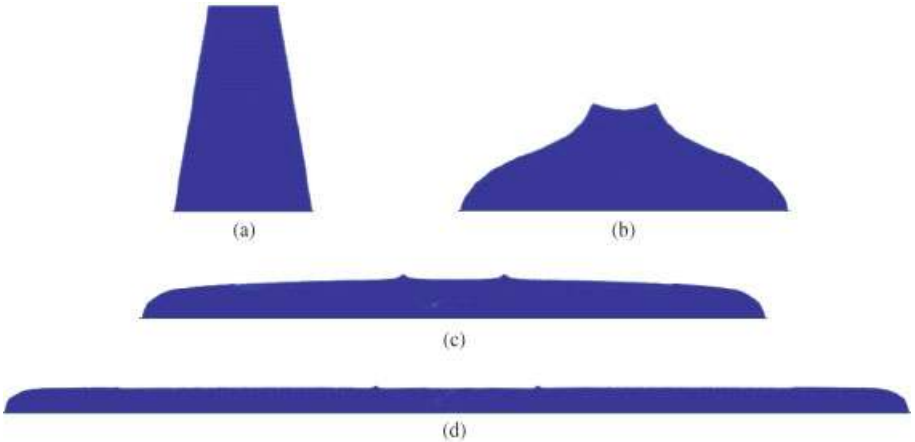

Figure 7. Different snapshots of the slump test on SCC at time: (a) 0 s; (b) 0.36 s; (c) 1.87 s; and (d) 7.24 s.

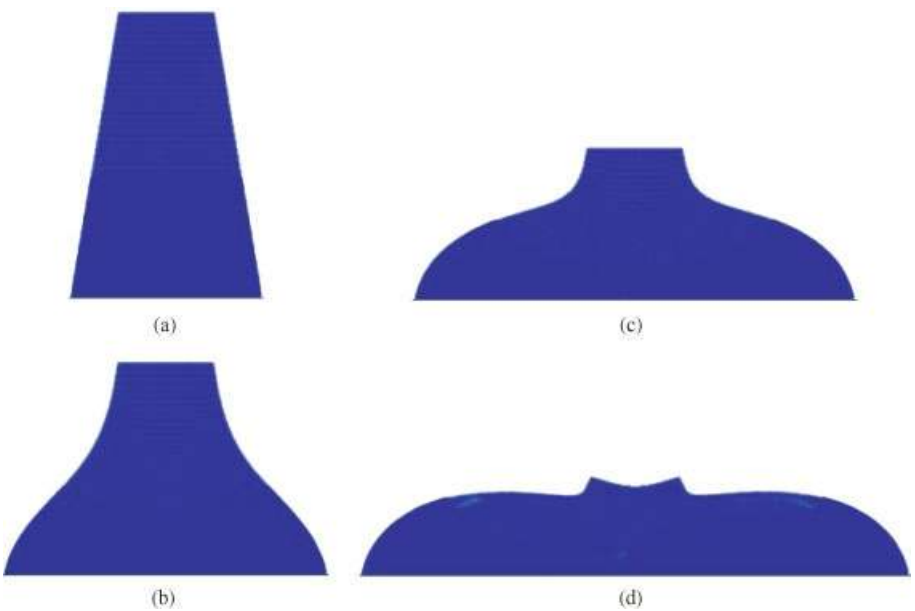

Figure 8. Different snapshots of the slump test on HPC at time: (a) 0 s; (b) 0.3 s; (c) 0.87 s; and (d) 5.56 s.

set up, on one hand, the air viscosity to one-tenth of this value and, on the other hand, the maximum viscosity of concrete to 10^3 times this value. The maximum viscosity is used to limit the viscosity of the modified Bingham's model for a shear strain rate close to zero. Parametric studies have shown that results are not significantly influenced by these choices, compared to computations with a constant, realistic, viscosity of air.

Figures 7 and 8 represent different snapshots of the flow during a slump test for the SCC and the HPC, respectively. They show the difference in fluidity between these two concretes.

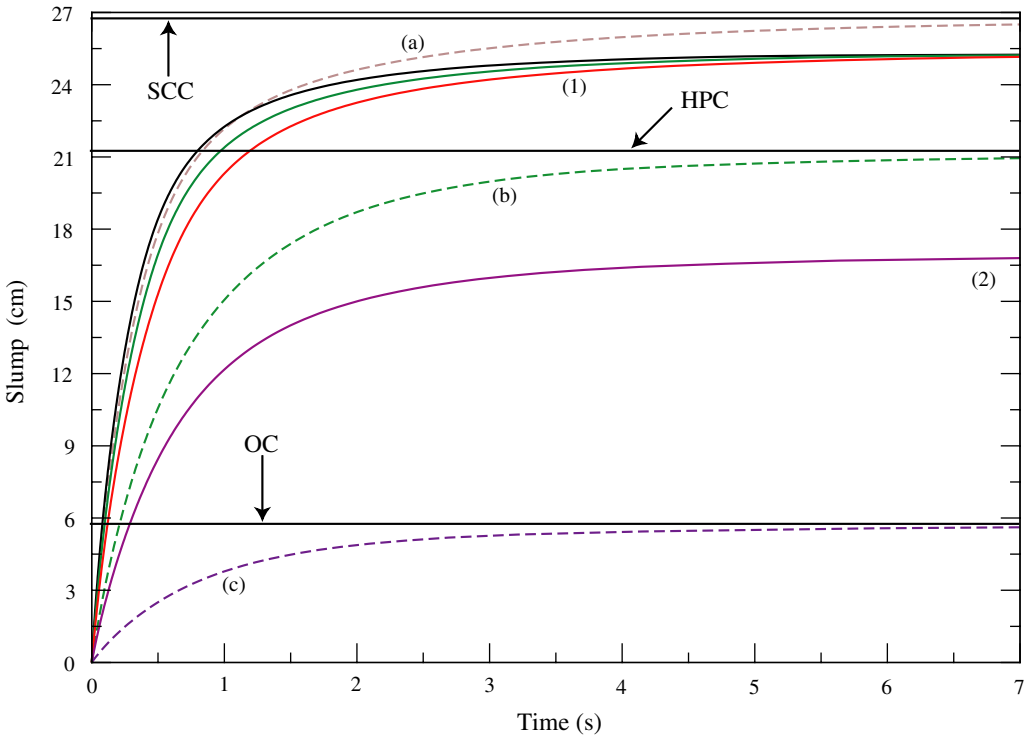

Figure 9. Slump of concrete with the Abrams cone test after Bingham's parameters identification for OC (c), HPC (b) and SCC (a). The plain line correspond to the numerical results using *Bétonlab*'s parameters for HPC (2) and SCC (1). There are three different lines for (1) which correspond to three different plastic viscosity at the same yield stress.

Numerical results of the trial and error approach used to calibrate the Bingham's model are summarized in Figure 9. They show that in order to get the same slump as the one observed experimentally, the yield stress of the three different concretes needs to be 1900, 600 and 200 Pa for OC, HPC and SCC, respectively. Furthermore, in Figure 9 the slump evolution obtained for three different plastic viscosity with SCC is plotted for one given yield stress (292 Pa). We observe that the final slump is not affected by the plastic viscosity. In these computations, the plastic viscosity given by the concrete formulation software *Bétonlab* has been used.

3.3. Comparison with Bétonlab

The two Bingham's parameters could be calibrated from the above slump tests in which concrete flow is measured at different timesteps and inverse analysis using the above simulations. These two parameters could also be estimated from the composition of concrete and it may be interesting to compare results. We used for this the software *Bétonlab* [17] developed at LCPC[¶] in France. *Bétonlab* is based on the compressible packing model [7]. This model is summarized

[¶] Laboratoire Central des Ponts et Chaussées.

as follows: concrete is initially considered as a dry assembly of granular material with different grain classes (i). The proportion (y_i) and individual size distribution of each granular class are known. Firstly, the packing density (γ_i) of each class, as part of the whole material, is derived from the theoretical virtual packing density (β_i) taking into account wall effects and loosening effects due to other classes. (β_i) is a granular class property measured experimentally. (γ_i) is the maximum packing density attainable for the considered material with an infinite amount of compaction energy. Secondly, concrete is considered as a suspension of a solid skeleton in water. By analogy with some viscosity models, a compaction index (K') is defined from the compaction index of each solid skeleton (K'_i) by

$$K' = \sum_{i=1}^{n} K'_i = \sum_{i=1}^{n} \left(\frac{\frac{y_i}{\beta_i}}{\frac{1}{\Phi} - \frac{1}{\gamma_i}} \right) \tag{15}$$

where Φ is the solid content of the concrete (that is the complement to 1 of the water content). The plastic viscosity is then written as

$$\mu = \exp\left(A \times \left(\frac{\Phi}{\Phi^*} - B \right) \right) \tag{16}$$

where Φ^* is the packing density of the skeleton defined as the value of Φ which gives a compaction index of 9. A and B are two constants empirically evaluated on hundreds of tests. The yield stress is derived from the empirical formula

$$\tau_0 = \exp(a_0 + a_c K'_c + a_f K'_f + a_S K'_S + a_s K'_s + a_g K'_g + a_G K'_G) \tag{17}$$

a are empirical parameters depending on grain size and on superplasticizer quantity. These parameters are calibrated with the BT RHEOM developed by de Larrard *et al.* [6]. This BT RHEOM is a parallel-plate rheometer where the strain field is imposed by the geometry. From the relation between the torque and the rotation speed, one can deduce the material law of behaviour. Index c is related to cement, f to calcareous filler, s to powders with grains smaller than 80 μm, S to sand grains, g to small aggregates and G to larger aggregates.

The Bingham's parameters predicted by *Bétonlab* for the three considered concretes are given in Table V. The difference with the calibration of the slump test results with *ellipsis* are also given in this table.

Mean errors on the plastic viscosity and the yield stress as predicted by the software *Bétonlab* are 50 Pa s and 148 Pa [19], respectively. These errors are due to the non-repeatability of the experimental procedure used for calibrating the formula (Equations (16) and (17)) because of material heterogeneities, but they may depend on the type of rheometer used.

Table V. Bingham's parameters output from Bétonlab.

	OC	HPC	SCC
Plastic viscosity (Pa s)	431	390	244
Yield stress (Pa)	1864	897	292
Numerical calibration	1900	600	200
Error with calibration results (%)	2	33	32

Table VI. Bingham's parameters output from Bétonlab.

Viscometer	Properties	1	2	3	4	5
BML	Slump (cm)	9.0	17.0	21.5	23.0	26.5
	τ (Pa)	1310	519	0	34	173
	η (Pa s)	13	33	170	70	73
BT RHEOM	Slump (cm)	12.5	17.0	22.5	23.0	23.5
	τ (Pa)	1600	1190	306	747	721
	η (Pa s)	71	82	354	209	172

Hu [20] has compiled results from two studies done on five different concretes with different rheometers. The first one is the BML [21] and the second one is the BT RHEOM. A summary of results is presented in Table VI.

Fresh concrete is very sensitive at such an early age to time, temperature, humidity, mixing method, etc. Therefore even a simple test like the slump test shows quite a large variability if environmental conditions and testing are not always the same. Another conclusion from these data from literature is that BT RHEOM seems to over evaluate the yield stress as well as the plastic viscosity even for concrete with the same slump. The same conclusion can be drawn from our study for the yield stress solely as we did not focus on the plastic viscosity. In Figure 9, comparison between the calibration and the results from *Bétonlab* show that the second over evaluate the yield stress. A second comparison campaign on OC and HPC has been done between the BT RHEOM and the CEMAGREF-IMG [22]. This work does not show any tendency of one rheometer to always over estimate Bingham's parameters as in the first study by Hu [20]. The relative error stands between 3 and 56% for the yield stress and between 1 and 94% for the plastic viscosity which points out the great experimental dispersion on the determination of the two Bingham's parameters.

Regardless of error due to the 2D assumption, the numerical analysis of the slump test gives an estimation of the yield stress up to 2, 33 and 32% for OC, HPC and SCC, respectively, which is within the experimental dispersion. Considering the dispersion, one can use the shear stress threshold given by Equations (15) and (17) in numerical simulations at least for OC. As for the plastic viscosity, the lack of experimental data (e.g. snapshots during a slump test) and the relatively large dispersion between the data found in the literature leave the choice of a proper predicting formula rather open. We have used throughout this paper the values provided by Equation (16) in *Bétonlab*. Since we are interested in the final stage of the flow of concrete here, the consequences of a misevaluation of this parameter are not so important (as seen of Figure 9).

4. STUDY OF CONCRETE CASTING—LBOX TEST

The LBOX test is among the standard experiments aimed at measuring concrete workability. It is a formwork made of wood with a square column in which concrete is placed. The inner surface in contact with the test material is made of bakelite. A door at the bottom is opened and the material flows. Measurements consist in recording the arrival time at the end of the horizontal part and also the profile of the free surface of concrete in the horizontal part. Usually, vertical reinforcement bars are placed just after the door so that concrete has to flow in

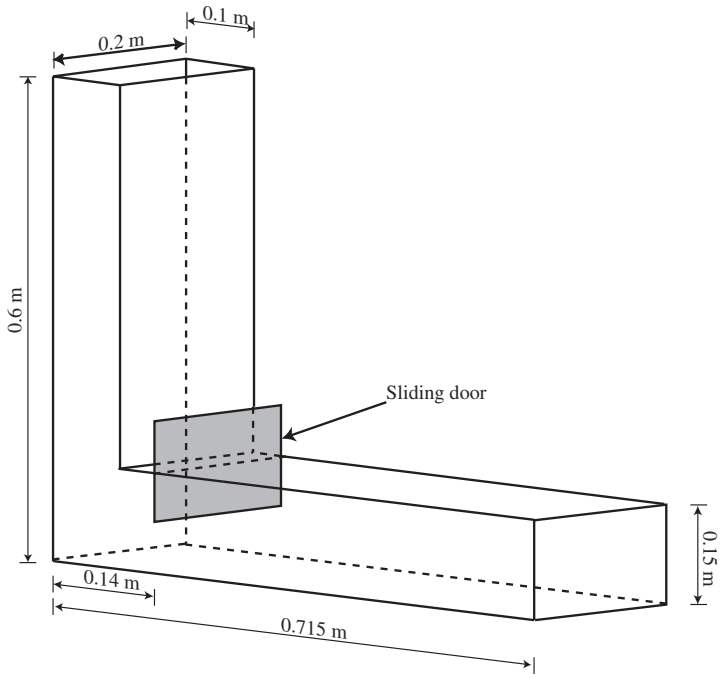

Figure 10. Geometry of the LBOX.

Table VII. Experimental results of the Lbox test for each concrete.

	Distance (cm)	0	10	20	30	40	50	End	Time (s)
SCC	Height (cm)	9.5	9.3	9.15	9.0	8.8	8.6	8.5	2.5
HPC	Height (cm)	13	9	7.5	6.8	6	4.5	3.5	11

between them. In the present application, those bars have been removed since they cannot be modelled in a 2D simulation. Figure 10 shows the geometry of the LBOX. In the 2D computation a unit thickness of material is described.

4.1. Experimental study

We did not perform the Lbox test for OC as we do not expect any flow due to the large yield stress. For each test we measured the arrival time of the material at the other end of the box and once the flow was completed we measured in seven different cross sections of the horizontal part of the LBOX the concrete height. The first cross section is the door section and the six others follow at a distance of 10, 20, 30, 40, 50 and 57 cm from the door. The furthest section corresponds to the end of the LBOX. Experimental results are summarized in Table VII.

Due to the hydrostatic pressure generated by concrete, we had some difficulties in opening the door during experiments identically every time from one test to another. The consequence is that the variation for the opening time may not be negligible in the computations as we will see next.

4.2. Numerical modelling

We used a mesh of four levels and 12×12 elements at the coarsest level which means 9216 elements overall. The mesh was slightly refined on the left and at the bottom parts of the grid where material flow takes place (Figure 11). Same as for the slump test computation model, we used 36 particles per element for the concrete zone and nearby, and 16 particles per element in the air zone. Boundary conditions were always free-slip including for internal boundaries defining LBOX walls and door. The only driving force was gravity with a concrete density of 2.45. Due to difficulties encountered during experiments regarding the opening of the door, we used a moving internal boundary in order to model the door motion upward with a finite opening time. We recorded the evolution with time of concrete height in the cross sections where measurements were done. Results are shown in Figures 12 and 13 for SCC and HPC respectively. We present only results for four cross sections which correspond to the first, third, fifth and seventh cross section of measurements, respectively, for more clarity of the figures.

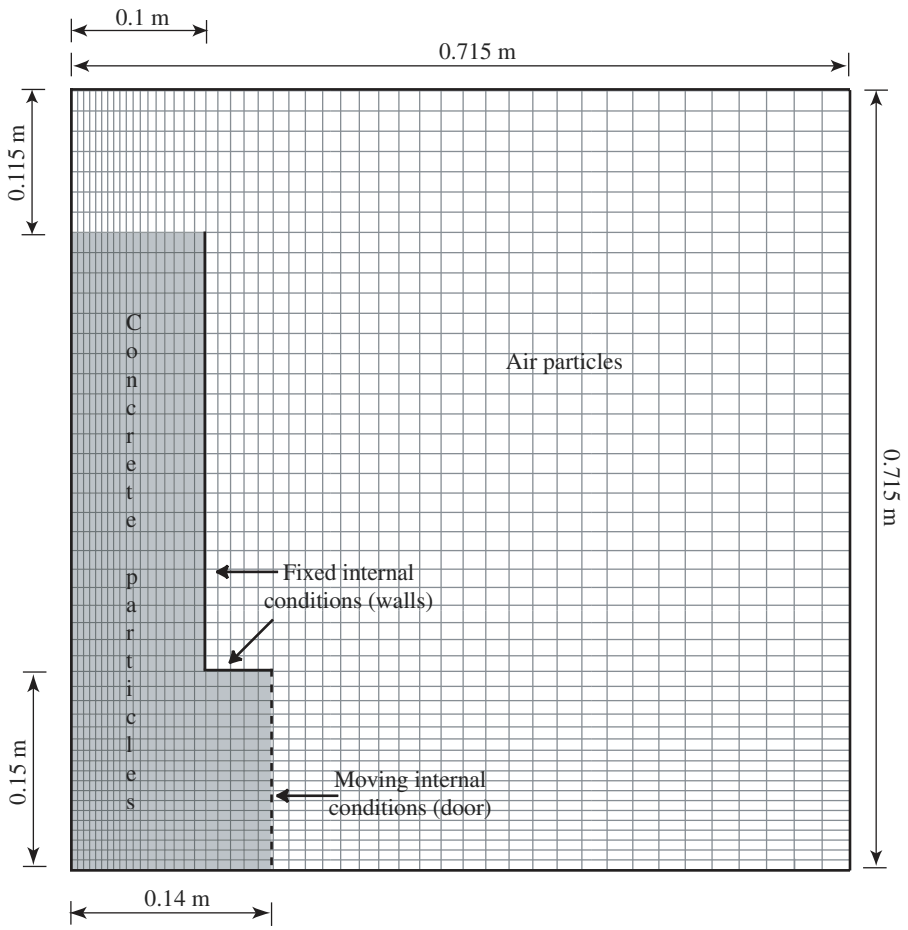

Figure 11. Mesh used in *ellipsis* for the Lbox problem. For the sake of clarity we show the mesh at level 3. The actual finest mesh used in this work is obtained by dividing each element in 4.

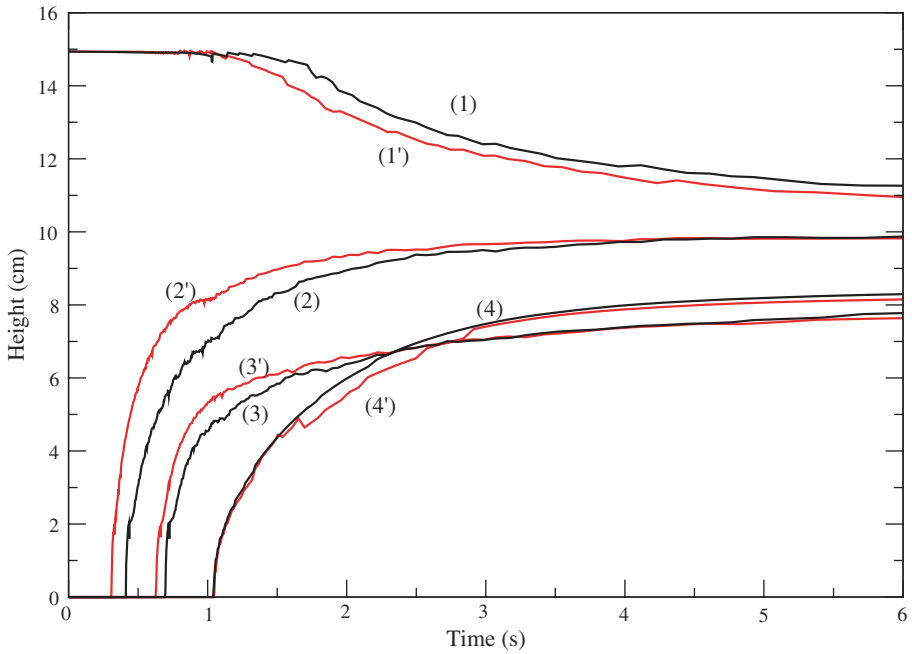

Figure 12. Evolution in time of concrete height in four different cross sections for SCC flow: (1) for the door cross section; (2) and (3) at a distance of 20 and 40 cm, respectively; and (4) for the end section. Curves with a ($'$) correspond to a door opening time of 1 s and others to 0 s.

Figures 14 and 15 show different snapshots of the SCC flow in the Lbox test for opening times of 0 and 1 s, respectively, and Figures 16 and 17 show different snapshots of the HPC flow for the same opening times.

One can see that the final stage, once concrete has reached static equilibrium, is very much dependent on the opening conditions in the LBOX test. Practically, it is quite difficult to measure the duration of the opening of the door in the experiments. An opening time of 1 s seems to be a quite realistic value from an experimental point of view.

We present in Table VIII the numerical results concerning HPC and SCC. The time at which concrete reaches the box end and the height of concrete in several cross sections for the final stage are provided. Same as for the slump test, the plastic viscosities of the two concretes provided by the software *Bétonlab* have been used in the computations. Comparisons with Table VII show a good agreement for the recorded heights of concrete. The flow time is quite well estimated within 15% for HPC. Regarding SCC, the flow time is so small that the experimental relative error on the duration of the concrete flow is very large.

5. CONCLUSIONS

We have presented in this paper a numerical model aimed at simulating concrete flow in formworks. This is a first step towards the development of a 3D simulation tool. Attention has

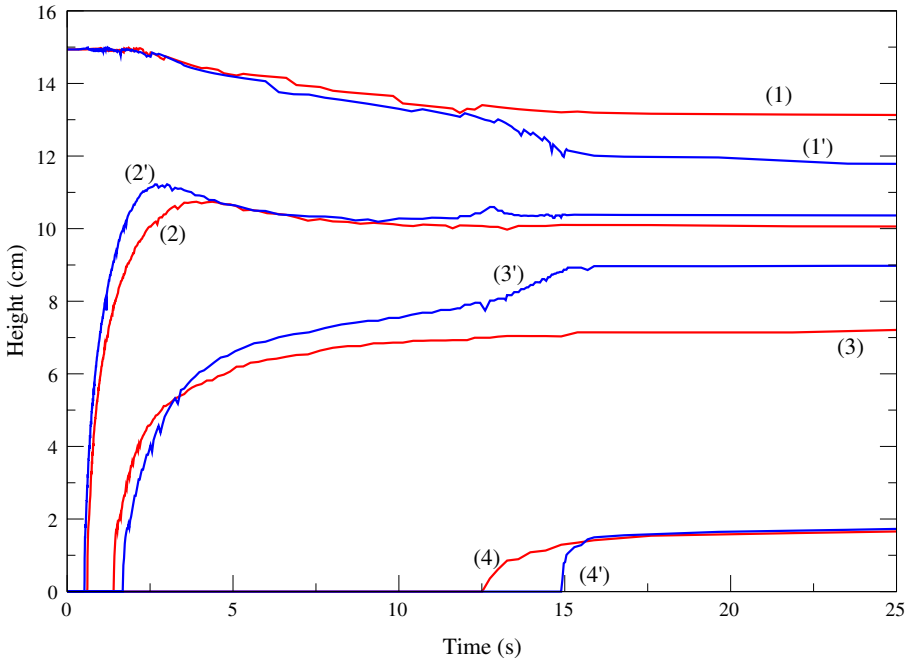

Figure 13. Evolution in time of concrete height in four different cross sections for HPC flow: (1) for the door cross section; (2) and (3) at a distance of 20 and 40 cm, respectively; and (4) for the end section. Curves with a ($'$) correspond to an door opening time of 1 s and others to 0 s.

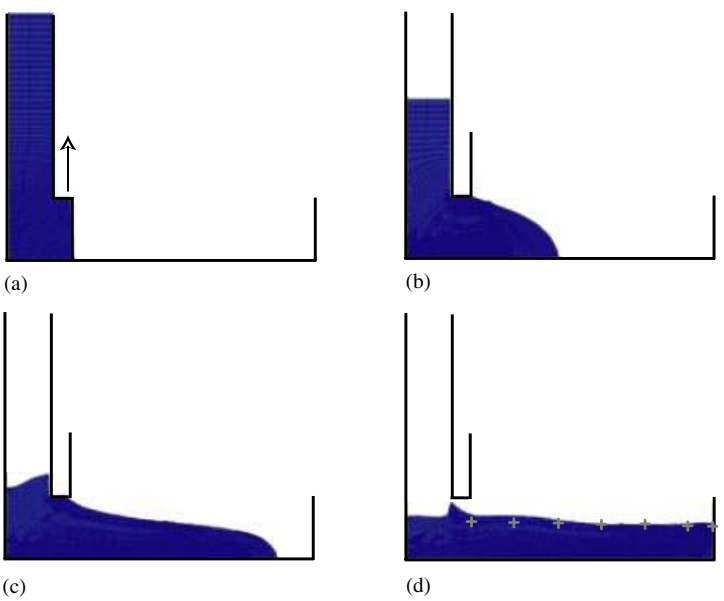

Figure 14. Different snapshots of the Lbox test on SCC at time: (a) 0 s; (b) 0.28 s; (c) 0.85 s; and (d) 31.9 s with an instantaneous door opening. Crosses represent experimental measurements.

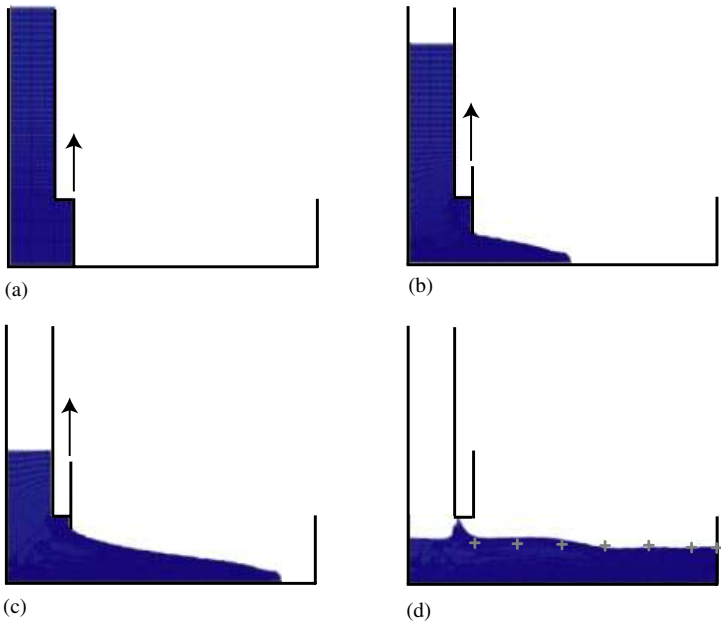

Figure 15. Different snapshots of the Lbox test on SCC at time: (a) 0 s; (b) 0.45 s; (c) 0.85 s; and (d) 7.63 s with a door opening time of 1 s. Crosses represent experimental measurements.

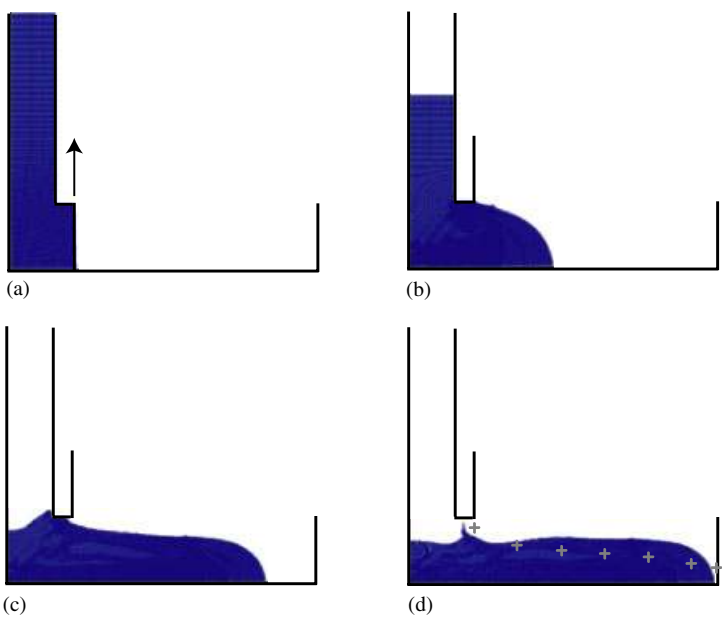

Figure 16. Different snapshots of the Lbox test on HPC at time: (a) 0 s; (b) 0.49 s; (c) 4.89 s; and (d) 49.5 s with an instantaneous door opening. Crosses represent experimental measurements.

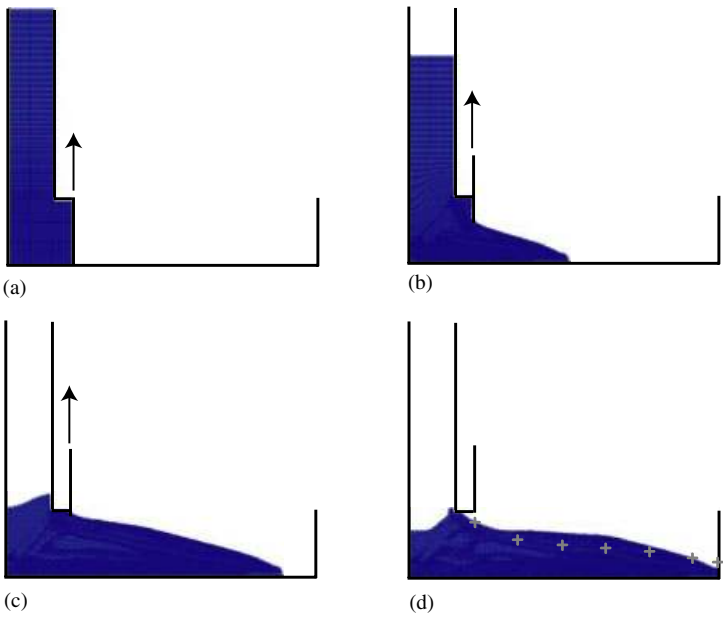

Figure 17. Different snapshots of the Lbox test on HPC at time: (a) 0 s; (b) 0.66 s; (c) 2.81 s; and (d) 47.3 s with a door opening time of 1 s. Crosses represent experimental measurements.

Table VIII. Numerical results of the Lbox test for each concrete.

	Distance (cm)	0	20	40	End	Time (s)
SCC	Height (cm)	10.5	9.8	7.6	8.1	1.1
	Error (%)	9.5	7.1	13.6	4.7	56
HPC	Height (cm)	13.1	10	7.1	1.8	12.5
	Error (%)	0.8	33.3	18.3	48.6	13.6

been focused first on the rheology of concrete. The simple Bingham's model has been chosen and the model parameters have been calibrated for several concretes, quite different from a rheological point of view. The shear stress threshold in the Bingham's model can be calibrated from a slump test and a quite consistent prediction is provided with empirical formula available in a concrete formulation software at least for OC. The plastic viscosity, however, needs a rheometer to be measured. We found that, according to the literature, the measurement of this model parameter is still very much dependent on the testing apparatus employed and a proper, objective experiment remains to be devised. Inverse analysis using the present simulation tool might be also envisioned.

Simulations on the LBOX experiment, in which a 2D flow is reproduced, are close to the experiments. Again, since the plastic viscosity has not been obtained from experiments, we used

the value provided by the concrete formulation software and compared the final stages of the concrete flow only.

This study mainly shows that one can use the FEMLIP to model concrete flow with an homogeneous approach. Several simplifying assumptions have been made. The boundary conditions between the formworks and concrete are assumed to be perfect, without friction. Sensitivity analyses have been performed which show that friction is not very important, compared to the influence of the dispersion in the experimental determination of the plastic flow especially. In the LBOX test errors may also be due to the wall effect in the perpendicular direction of the plane of study. Indeed the width of the LBOX is not large enough to neglect wall effects. 3D computations and simulations of concrete flow viewed as a heterogeneous fluid are currently in progress in order to assess these assumptions and to provide tools which are capable detecting possible segregation and blocking of aggregates during casting of concrete.

ACKNOWLEDGEMENTS

Authors would like to acknowledge Dr Philippe TURCRY for his fruitful help during this work, in particular, for the concrete formulation and experimental parts.

REFERENCES

1. Moresi L, Dufour F, Mühlhaus H-B. Mantle convection models with viscoelastic/brittle lithosphere: numerical methodology and plate tectonic modeling. *Pure and Applied Geophysics* 2002; **159**:2335–2356.
2. Petersson Ö. Simulation of self-compacting concrete—laboratory experiments and numerical modelling of testing methods, jring and l-box tests. In *Proceedings of the 3rd International RILEM Symposium*, *Pro 33*, Wallevik O, Nielsson I (eds). RILEM: Cachan, 2003; 202–207.
3. Noor MA, Uomoto T. Three-dimensional discrete element simulation of rheology tests of self-compacting concrete. In *Proceedings of the 1st International RILEM Symposium on Self-Compacting Concrete*, Skarendahl Å, Petersson Ö (eds). RILEM: Cachan, 1999; 35–46.
4. Mühlhaus H-B, Dufour F, Moresi L. A director theory for visco-elastic folding instabilities in multilayered rock. *International Journal of Solids and Structures* 2002; **39**:3675–3691.
5. Yahia A, Khayat KH. Applicability of rheological models to high-performance grouts containing supplementary cementitious materials and viscosity enhancing admixture. *Materials and Structures* 2003; **36**:402–412.
6. Tatersall GH. The rationale of a two-point workability test. *Magazine of Concrete Research*, 1973; **25**(84): 172–179.
7. de Larrard F, Ferraris CF, Sedran T. Fresh concrete: a Herschel–Bulkley material. *Materials and Structures* 1998; **31**(211):494–498.
8. Ferraris CF, de Larrard F. Testing and modelling of fresh concrete rheology. *NISTIR 6094*, February 1998; 59.
9. Tsong Y, Chao-Wei T, Chao-Shun C, Kuang-Hong C. Flow behaviour of high strength high-performance concrete. *Cement and Concrete Composites* 1999; **21**(5–6):413–424.
10. Papanastasiou TC. Flows of materials with yield. *Journal of Rheology* 1987; **31**:385–404.
11. Ukraincik V. Study of fresh concrete flow curves. *Cement and Concrete Research* 1980; **10**:203–212.
12. Moresi LN, Solomatov VS. Numerical investigation of 2d convection with extremely large viscosity variations. *Physics of Fluids* 1995; **7**(9):2154–2162.
13. Moresi L, Dufour F, Mühlhaus H-B. A Lagrangian integration point finite element method for large deformation modeling of viscoelastic geomaterials. *Journal of Computational Physics* 2003; **184**(2):476–497.
14. Dufour F, Moresi L, Mühlhaus H-B. Modelling solid particles suspended in a viscous fluid. In *Proceedings Chapman Conference on Exploration Geodynamics*, Moresi L, Müller D (eds). American Geophysical Union, 2001; 124–136.
15. Bramble JE, Pasciak JH, Vassilev AT. Analysis of the inexact Uzawa algorithm for saddle point problems. *SIAM Numerical Analysis* 1997; **34**:1072–1092.
16. Cahouet J. Chabard J-P. Some fast 3d finite element solvers for the generalized Stokes' problem. *International Journal for Numerical Methods in Fluids* 1988; **8**:869–895.
17. de Larrard F, Fau D. *Bétonlab*: *logiciel d'aide à la formulation des bétons*. Presses de l'ENPC: Paris, 1992.
18. de Larrard F, Szitkar JC, Hu C. Design of a rheometer for fluid concretes. In *RILEM Workshop Special Concretes*: *Workability and Mixing*, E&FN Spon. Kluwer Academic Publishers: London, 1993; 201–208.

19. Sedran T, de Larrard F. Optimization of self compacting concrete thanks to the packing model. In *Proceedings of the 1st International RILEM Symposium on Self-Compacting Concrete*, Skarendahl Å, Petersson Ö (eds). RILEM: Cachan, 1999; 321–332.
20. Hu C. Rhéologie des bétons fluides. *Série ouvrages d'art OA 16*, Laboratoire des Ponts et Chaussées, 1995.
21. Wallevik OH, Gjorv OE. Development of a coaxial cylinders viscometer for fresh concrete. *Proceedings of the International Conference on* '*Properties of Fresh Concrete*'. RILEM, Chapman & Hall: London, 1990; 213–224.
22. Coussot P. Rhéologie des boues et laves torrentielles—Etudes des dispersions et suspensions concentrées. *Ph.D. Thesis*, Institut National Polytechnique de Grenoble, 1993.